Near-Critical Phenomena and Resolution in Supercritical Fluid Chromatography

The analysis in this paper shows the relationship between molecular resolution in supercritical fluid chromatography (SFC), and certain divergent thermodynamic properties of solutes dissolved in near-critical fluids. This divergence is most pronounced in the near-critical regime, leading to the hypothesis that this region provides most promise for heightened molecular resolution, which lies at the heart of analytical and separation technologies.

A thermodynamic model for representing capacity factor data in SFC is proposed, spanning a wide density range. The model uses a perturbed hard sphere equation for the fluid phase and lattice concepts for the stationary phase. In addition, data are presented for a number of systems and discussed in terms of the analysis provided. For an isomeric system, the data shows that resolution between species increases with the onset of retrograde behavior, resulting in a distinct maximum point.

F.D. Kelley
E.H. Chimowitz
Department of Chemical Engineering
University of Rochester
Rochester, NY 14627

Introduction

Supercritical fluid chromatography (SFC) has generated considerable interest in recent years as a potentially attractive molecular separations technique. The often cited advantages of supercritical fluids, such as the ability to "tune" solvent strength with small pressure and/or temperature changes, low-temperature processing, ease of solvent regeneration, and nontoxicity of fluids like carbon dioxide make SFC a credible alternative to more established methods such as HPLC. There have been many papers on SFC in the recent past, primarily in the analytical chemistry literature on an extremely wide class of molecular systems ranging from oligomeric separations to the analysis of biologically active compounds. Much of the published data are for the relatively high density region of the supercritical fluid. The main reason for this is that solute loadings in the supercritical phase generally increase with solvent density; particularly for compounds of high molecular weight and low volatility this can be an important consideration. The thermodynamic modeling of the dense supercritical fluid region, as opposed to the highly compressible near-critical region, can also be done more accurately with an equation of state approach, as discussed by Wong et al. (1985).

The focus of this work is the highly compressible near-critical region, where theory is much less successful and for which chromatographic data are more scarce. An early review paper by Van Wasen et al. (1980) pointed out unusual behavior of equilibrium partition coefficients in the near-critical region. More recent works also show interesting features of data in this region (Yonker et al., 1987; Shim and Johnston, 1989); in particular, papers by Schmitz et al. (1984) and Klesper and Schmitz (1988) provide striking evidence of the highly nonlinear behavior of equilibrium coefficients with respect to pressure and temperature variations, as the critical point of the fluid phase is approached or traversed.

In the near-critical region of a supercritical fluid in contact with a solute, one interesting property of the system is the existence of retrograde behavior. This has been the subject of a number of our recent papers and those of others, (Chimowitz et al., 1988; Kelley and Chimowitz, 1989; Debenedetti and Kumar, 1988; Johnston et al., 1987; Schaeffer et al., 1988). The allied crossover effect phenomenon, a situation in which certain components in the system are retrograde while others are not, was proposed by Chimowitz and Pennisi (1986) as the basis for novel molecular separation techniques using a staged processing concept. A single-step, high-purity isolation technique based upon these ideas was demonstrated to be feasible (Kelley and Chimowitz, 1989) in a model system consisting of benzoic acid, 1-10 decanediol dissolved in supercritical carbon dioxide.

The staged concept has limitations, discussed by Kelley and Chimowitz. The purpose here is to present a thermodynamic analysis and data for fixed-bed operations using near-critical

mobile phases. The uses of fixed beds with supercritical phases have a number of technological applications, ranging from the regeneration of activated carbon adsorption beds (Recasens et al., 1989) to supercritical fluid chromatography. The behavior of the solute species when the mobile phase is near-critical is strongly dependent upon pressure, temperature, and density. A number of striking features of the experimental data have been recognized, including the existence of retention time maxima and linear capacity factor density relationships over limited density ranges (Klesper and Schmitz, 1988; Chimowitz and Kelley, 1989). However, we believe an adequate explanation of the thermodynamic basis for these phenomena has not been published to the present. We show that it is the divergent nature of particular thermodynamic properties in near-critical systems (for example, the singularity in the infinite dilution solute partial molar enthalpy function at the critical point) that is central to understanding system behavior. This divergence and retrograde phenomena in near-critical systems are closely related. This perspective is developed and new data are presented to support this viewpoint.

Thermodynamics of the Surface Species, Near-Critical Fluid Interaction

In order to carry out this analysis in terms of standard chromatographic terminology we consider the capacity factor k_i, for species i.

For linear chromatography (germane to the systems we consider since they are extremely dilute) k_i is defined (per unit bed volume) as:

$$k_i = \frac{\text{number of moles of } i \text{ in the stationary phase}}{\text{number of moles of } i \text{ in the mobile phase}}$$

By further defining q_i^*as the solid-phase concentration of species adsorbed in the stationary phase (moles per unit mass), y_i as its mole fraction in the mobile phase, ρ_B as the bulk density of the solid phase as packed (mass of solid phase divided by volume of bed), ϵ as the bed porosity, and ρ_m as the molar density of the mobile phase, k_i may be expressed as:

$$k_i = \frac{\rho_B q_i^*}{\epsilon y_i \rho_m} \tag{1}$$

where the quantity $q_i^*/y_i\rho_m$ is the thermodynamic adsorption equilibrium constant, also known as the partition coefficient for species i. Capacity factors and adsorption equilibrium constants are thus closely related, and in fact are identical except for the factor ρ_B/ϵ, dependent only on the bed's physical structure. For isothermal dilute systems the dynamic equations of convective and interphase transport in the bed can be solved (Sherwood et al., 1975), yielding the following useful result:

$$k_i = \frac{\tau_i - \tau_0}{\tau_0} \tag{2}$$

Here τ_i is the mean residence time of species i in the column and τ_0 is the residence time of an unretained species. This is an important result since it enables capacity factors to be determined experimentally by measuring mean residence times of the species. By nondimensionalizing time in this manner, the capacity factor reflects the inherent thermodynamic partitioning of the species between phases. Nonthermodynamic effects, which contribute to solute retention time—column length, for example—are factored out.

Given these definitions we are in a position to pursue the objective of determining the effects of temperature and pressure on solute capacity factors. The analysis is done for a binary mobile phase in contact with a stationary phase with a fixed number of adsorption sites per mole of packing material. Both solute and carrier molecule adsorption are permitted.

By utilizing the differential approach to phase equilibrium along the saturation envelope (Modell and Reid, 1983) the following equations relating fugacity in each phase pertain (b refers to the solute, a to the solvent):

$$d \ln f_b^m = d \ln f_b^s$$

and

$$d \ln f_a^m = d \ln f_a^s$$

These derivatives can be expanded in terms of the usual intensive variables for each phase yielding:

$$-\left[\frac{(\bar{h}_a^m - h_a^o)}{RT^2} + \frac{(\bar{h}_a^s - h_a^o)}{RT^2}\right] dT + \left[\frac{\bar{v}_a^m - v_a^s)}{RT}\right] dp + \left(\frac{\partial \ln f_a^m}{\partial y_b}\right)_{p,T} dy_b - \left(\frac{\partial \ln f_a^s}{\partial \theta_a}\right)_{p,T,\theta_b} \mathrm{d}\theta_a - \left(\frac{\partial \ln f_a^s}{\partial \theta_b}\right)_{p,T,\theta_a} d\theta_b = 0 \tag{3}$$

for the solvent, and

$$\left[-\frac{(\bar{h}_b^m - h_b^o)}{RT^2} + \frac{(\bar{h}_b^s - h_b^o)}{RT^2}\right] dT + \left[\frac{\bar{v}_b^m - v_b^s)}{RT}\right] dp + \left(\frac{\partial \ln f_b^m}{\partial y_b}\right)_{p,T} dy_b - \left(\frac{\partial \ln f_b^s}{\partial \theta_a}\right)_{p,T,\theta_b} \mathrm{d}\theta_a - \left(\frac{\partial \ln f_b^s}{\partial \theta_b}\right)_{p,T,\theta_a} d\theta_b = 0 \tag{4}$$

for the solute. The variables θ_i refer to the coverage fraction of species i in the stationary phase, and superscript o means the ideal gas reference state.

Since in this paper we are primarily interested in the effect of temperature on capacity factors, p and y_b are considered constant in Eq. 3, which can be rearranged to solve for $d\theta_a$. The result is:

$$d\theta_a = -\frac{\dfrac{(\bar{h}_a^m - \bar{h}_a^s)}{RT^2} dT + \left(\dfrac{\partial \ln f_a^s}{\partial \theta_b}\right)_{p,T,\theta_a} d\theta_b}{\left(\dfrac{\partial \ln f_a^s}{\partial \theta_a}\right)_{p,T,\theta_b}} \tag{5}$$

The approximation that the mobile-phase composition remains constant ($dy_b = 0$) for variations in T and p on the phase envelope is pertinent to SFC, where the mobile phase is very dilute; $y_b \approx 0$ and $dy_b \approx 0$ can be assumed for all variations in T and p. In the limit of infinite dilution, the condition $dy_b = 0$ becomes exact.

Using Eqs. 3, 4, and 5 it can be shown easily that the temperature derivative of the capacity factor is given by:

$$\left(\frac{\partial \ln k_b}{\partial T}\right)_{p,y_b} = \frac{[C_b(\overline{h}_b^s - \overline{h}_b^m) + C_a(\overline{h}_a^s - \overline{h}_a^m)]}{RT^2} + \alpha_m \quad (6)$$

The pressure derivative is given by:

$$\left(\frac{\partial \ln k_b}{\partial p}\right)_{T,y_b} = \frac{[C_b(\overline{h}_b^m - \overline{v}_b^s) + C_a(\overline{v}_a^m - \overline{v}_a^s)]}{RT} - \beta_m \quad (7)$$

Coefficients C_a and C_b are functions of the stationary phase fugacity derivatives with respect to θ_a and θ_b, and α_m and β_m are respectively the volume expansivity and isothermal compressibility of the mobile phase. The relationships for C_a and C_b are given by:

$$C_a = \frac{\frac{-1}{\theta_b}\left(\frac{\partial \ln f_b^s}{\partial \theta_a}\right)_{p,T,\theta_b}}{\Delta} \quad (8)$$

$$C_b = \frac{\frac{-1}{\theta_b}\left(\frac{\partial \ln f_a^s}{\partial \theta_a}\right)_{p,T,\theta_b}}{\Delta} \quad (9)$$

with

$$\Delta = \left[\left(\frac{\partial \ln f_b^s}{\partial \theta_b}\right)_{p,T,\theta_a}\left(\frac{\partial \ln f_a^s}{\partial \theta_a}\right)_{p,T,\theta_b} - \left(\frac{\partial \ln f_b^s}{\partial \theta_a}\right)_{p,T,\theta_b}\left(\frac{\partial \ln f_a^s}{\partial \theta_b}\right)_{p,T,\theta_a}\right] \quad (10)$$

The determinant function Δ in the denominator of Eqs. 8 and 9 is positive for a stable phase, as shown by Chimowitz et al. (1988). To evaluate this function we need a thermodynamic model for the stationary phase, itself a complicated phase consisting of solute, solvent, and packing molecules. A convenient theoretical framework for this purpose is provided by lattice-based theory, particularly because the molecule–site energy interaction, which is of central interest, enters neatly into the lattice partition function description (Hill, 1962). Using the usual lattice partition function defined as:

$$Q(T,M,N_1,N_2,\ldots,N_L) = \Omega(M,N_1,N_2,\ldots,N_L)\,\Pi_{i=1}^{L} q_i^{N_i} \quad (11)$$

where q_i is the bound molecule partition function and Ω is the configurational degeneracy, it is possible in principle to calculate the chemical potential and other thermodynamic properties of the bound species. The details of the model are provided in the Appendix for the case of Langmuirian adsorption. This allows formal evaluation of the derivatives in Eqs. 8 and 9 for use in Eq. 6. The final result is quite simple and is given by:

$$\left(\frac{\partial \ln k_b}{\partial T}\right)_{p,y_b} = (1-\theta_b)\frac{(\overline{h}_b^s - \overline{h}_b^m)}{RT^2} - \theta_a\frac{(\overline{h}_a^s - \overline{h}_a^m)}{RT^2} + \alpha^m \quad (12)$$

The two energy terms in Eq. 12 can be grouped into what is referred to as an enthalpy of transfer term denoted by $\Delta\overline{H}_b^{trans}$. For the general case of L adsorbing species this term is given by:

$$\Delta\overline{H}_b^{trans} = (\overline{h}_b^s - \overline{h}_b^m) - \sum_{i=1}^{L}\theta_i(\overline{h}_i^s - \overline{h}_i^m) \quad (13)$$

Equation 12 now becomes the compact expression given by:

$$\left(\frac{\partial \ln k_b}{\partial T}\right)_{p,y_b} = \frac{\Delta\overline{H}_b^{trans}}{RT^2} + \alpha^m \quad (14)$$

This enthalpy of transfer term is closely related to the enthalpy change per molecule of solute as it moves from the mobile to the stationary phase. It is of interest to note that our Eq. 12 taken at the infinite dilution reference condition for the solute, and with no solvent adsorption, is formally identical to the equation used by Brown et al. (1987) in their work. This is not surprising since Brown et al. treated the stationary phase as a mixture in which Henry's law applied to the solute species. From a thermodynamic and mathematical standpoint this is equivalent to single-solute Langmuirian adsorption in the diulte region. In related work, Yonker et al. (1985, 1987) proposed a model and interpretation of the factors governing retention in SFC. Here we discuss a number of features of their analysis. Their equations do not account for solvent adsorption, which is a potentially significant feature of the problem (see the second term in Eq. 12). In fact, without accounting for solvent adsorption it is difficult to explain the data of Schmitz et al. (1984), where capacity factors under virtually identical conditions for a number of solutes dissolved in *i*-butane and *n*-butane are significantly different. In addition, we disagree with the statement that their equivalent of Eq. 14 at infinite dilution is valid only over a limited temperature range far from the critical point. The basis for these equations embodies fundamental chemical thermodynamics, and as a result they are valid over all temperature ranges even at the critical point where the term $\overline{h}_b^m$ at infinite dilution diverges according to an exact relationship (Debenedetti and Kumar, 1988). Because of this divergence in the partial molar energy functions for the solute in the neighborhood of the critical point, Yonker et al. (1987) proposed replacing the quantity $\Delta\overline{H}_b^{trans}$ by a heat capacity equivalent given as $\Delta H_b^{\infty} = \Delta\overline{H}_b^{\infty}(T_0) + \int_{T_0}^{T_f}\Delta\overline{C}_{pb}^{\infty}\,dT$. This, however, requires a value for $\Delta\overline{H}_b^{\infty}(T_0)$, which, if $T_0 = T_c$ (a valid choice), diverges to infinity and leaves unanswered the question of how to obtain $\overline{C}_{pb}^{\infty}$. Yonker et al. proposed approximating this term by the heat capacity of the mobile phase, but the two quantities are not equivalent. There is no need to take this route since the solute energy functions in Eq. 12 are directly available from a suitable equation of state. Such equations have been studied recently (Debenedetti and Kumar, 1988; Chimowitz et

al., 1988), and the energy functions predicted preserve the singularity at the critical point and are quite representative of the features of data for near-critical systems where these have been measured experimentally (Casielles et al., 1988). The importance of retaining the correct $(\bar{h}_b^m - h_b^0)$ functional dependence on pressure and temperature (including the singularities at the critical point) cannot be overstated. Indeed our analysis shows that it is the very nature of this strong dependence that is responsible for the interesting behavior of capacity factors that we next discuss.

SFC Retrograde Effect and Capacity Factors: Qualitative Model Interpretation

The analysis in the preceding section enables us to explore, at least qualitatively, the factors affecting retention time with near-critical mobile phases. We attempt to draw the analogy between retrograde phenomena in solubility studies discussed in our previous work (Chimowitz et. al., 1988) with the situation in SFC. Equation 12 can be reformulated in terms of partial molar configurational enthalpy functions as:

$$\left(\frac{\partial \ln k_b}{\partial T}\right)_{p,y_b} = \frac{(1-\theta_b)}{RT^2}\left[(\bar{h}_b^s - \bar{h}_b^o) - (\bar{h}_b^m - h_b^o)\right] - \theta_a\left[(\bar{h}_a^s - \bar{h}_a^o) - (\bar{h}_a^m - h_a^o)\right] + \alpha^m \quad (15)$$

The surface species functions $\bar{h}_i^s - h_i^o$ are analogous to the usual heats of adsorption. The mobile phase functions $(\bar{h}_i^m - h_i^o)$ have been studied by Chimowitz et al. (1988) for near-critical mobile phases, where it was shown that the solute residual partial molar enthalpy function is the dominant quantity. This suggests that the strongest factor determining the variation of k_b with temperature in Eq. 15 is the solute term given as:

$$(h_b^o - \bar{h}_b^m) - \Delta H_b^{ads} \quad (16)$$

where ΔH_b^{ads} is defined as,

$$\Delta H_b^{ads} = h_b^o - \bar{h}_b^s \quad (17)$$

The condition for retrograde solubility behavior in pure solute–fluid systems provided by Chimowitz et al. (1988) is the satisfaction of the following inequality

$$(h_b^o - \bar{h}_b^m) > H_b^{sub} \quad (18)$$

where ΔH_b^{sub} is the heat of sublimation of pure solute at saturation. In SFC, since θ_b is small, the dominance of the solute functions suggests that Eq. 15 can be well approximated by

$$\left(\frac{\partial \ln k_b}{\partial T}\right)_{p,y_b} = \frac{[(h_b^o - \bar{h}_b^m) - \Delta H_b^{ads}]}{RT^2} + \alpha^m \quad (19)$$

For SFC, the analogous inequality to that shown in Eq. 18 is $h_b^o - \bar{h}_b^m > \Delta H_b^{ads}$, which we call the SFC inequality. The sign of this inequality determines the manner in which capacity factors change with temperature according to this analysis:

1. When this inequality is satisfied, k_b in Eq. 19 will increase, possibly dramatically, with increasing temperature. (For the mobile phases used here, α^m is positive.)

2. As the temperature continues to increase, the enthalpic term (numerator of the first term in Eq. 19) decays sharply and eventually becomes negative, violating the inequality condition. This means that the solute is no more in its compressible retrograde region. If this enthalpic term becomes negative enough, it may overcome the contribution by the thermal coefficient of expansion, α^m, in which case k_b will begin to decrease with temperature.

3. Because of the dominance and magnitude of the energetic effects in the retrograde region, any differences between molecules should be amplified here. Different molecules have different retrograde regions, making this area of the k_b–temperature map most interesting from an intrinsic molecular resolution standpoint. The basis for this conclusion follows from an analysis of the partial molar volume data at infinite dilution for solutes in supercritical fluids published by Eckert et al. (1986). Those data clearly show that different solutes in the same solvent can have strikingly large (and different) partial molar volumes at the same conditions of temperature and pressure. This is especially the case in the near-critical region. The same can be deduced about partial molar enthalpies since an exact relationship between these two quantities is given by $\bar{h}_i^\infty = T(\partial P/\partial T)_\sigma \bar{v}_i^\infty$ + a constant, where $T(\partial P/\partial T)_\sigma > 0$ is a pure solvent property evaluated at the solvent critical point. Hence $\bar{v}_i^\infty$ and $\bar{h}_i^\infty$ are closely connected. The enthalpy term is pivotal to the behavior of retention times, as discussed in the preceding analysis. The net result of this analysis is that capacity factors or equivalently adsorption equilibrium coefficients, with near-critical mobile phases, should behave in a bidirectional manner with temperature. That is, temperature should strongly influence the direction of interphase transfer with interesting technological implications. To test this hypothesis and some consequences, a series of experiments was planned.

Experimental Approach and Data Reduction

A diagram of the equipment used for determining capacity factors is shown in Figure 1. The carbon dioxide used in the experiments was obtained from Air Products Inc., and used without further purification. The gas cylinders were directly connected to the system using stainless steel flexible hoses lined with Teflon. A 2 μm filter was used to eliminate any particulate matter entrainment from the gas cylinders.

The pump and inlet reservoir were kept at approximately 0°C by an air bath. This low temperature ensured that liquid carbon dioxide was available at the pump inlet. A Milton Roy model 396-89 single piston pump was used.

The pressure throughout the system was controlled by a Tescom backpressure regulator, model 26-1724-24-043. The pressure at the outlet of the column was measured by a Heisse pressure gauge, Dresser Industries model CM-96619, with a range from 0 to 2,500 psig (0–172.4 bar). All the experimental data are reported using the outlet pressure of the system. The flow rates during the experiments were chosen to be low enough to maintain the pressure drop across the column at less than 2 bar at all times.

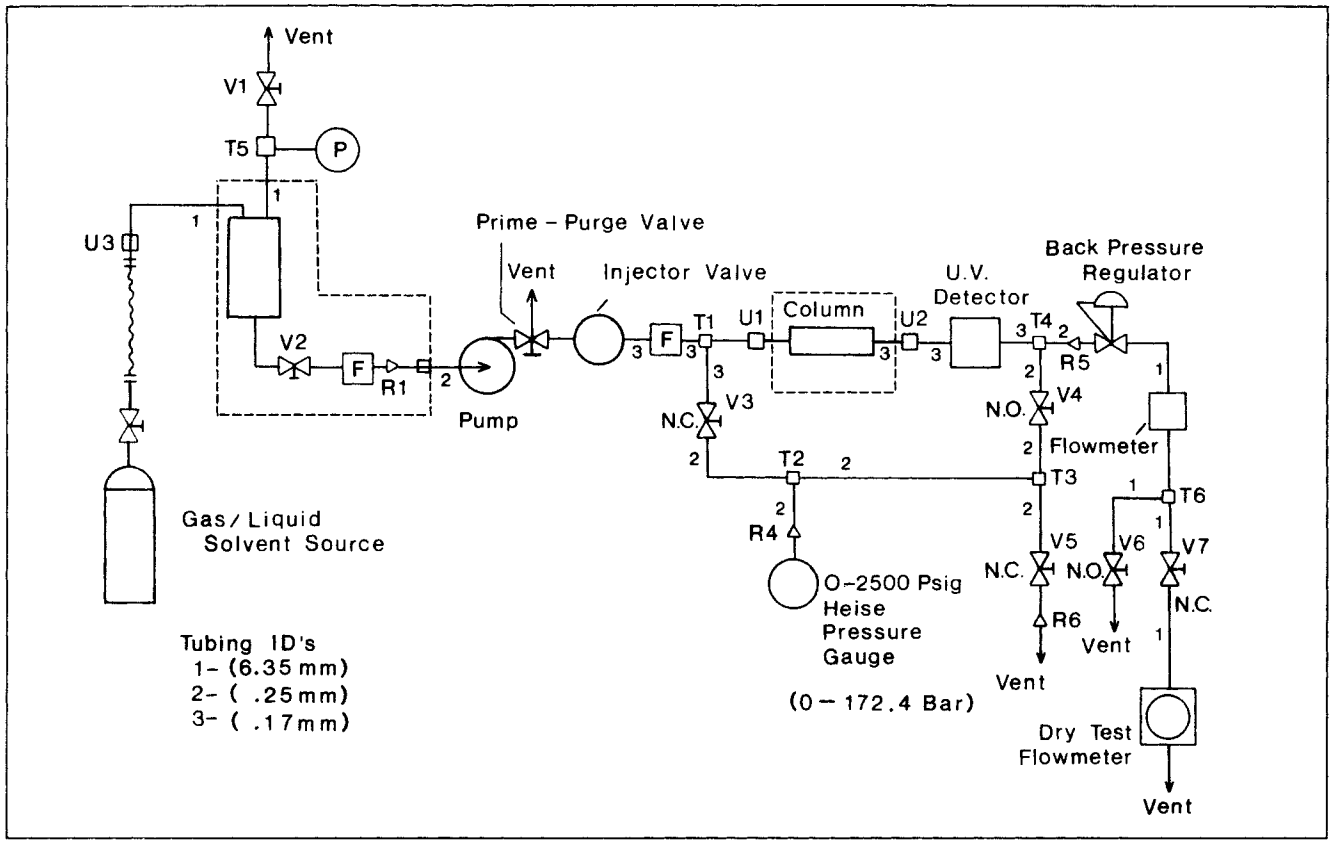

Figure 1. Experimental system for SFC data acquisition.

The flow rates through the system were obtained by measuring the time required for a known volume of gas to pass through a Singer model DTM-115 dry test meter. In general the flow rates of gas used were between 25.9 and 42.0 L/h. Stable flow rates that were less than approximately 22.0 L/h could not be maintained, since the Tescom backpressure regulator behaved erratically at very low flow rates. Flow rates in excess of approximately 85 L/h were not possible due to cavitation in the pump inlet check valves.

Dilute solutions of the solutes dissolved in hexanes (J. T. Baker Chemical Co.) or methylene chloride (Fisher Scientific Co.) were injected into the system by syringe through a Rheodyne model 7125 high-pressure injector valve. The valve sample loop was 20 μL. A magnetic switch (Rheodyne model 7150) on the injector valve sent a pulse to a microcomputer upon injection to initiate data accumulation. Solutes exiting the column were detected by a Water's model 440 UV detector, operated at a wavelength of 254 nm. The detector was unaltered for experimental use and was used successfully at system pressures as high as 2,300 psig, (158.5 bar).

The column used in this investigation was a Beckman Ultrasil ODS column, filled with 10 μm irregular particles. It was 25 cm long by 4.6 mm dia.

The solutes used were naphthalene (Mallinckrodt Chemical Works), 2,3-dimethylnaphthalene (Lancaster Synthesis), and 2,6-dimethylnaphthalene (Aldrich Chemical Co.). All solutes were used without further purification.

The columns were housed in the oven of a Hewlett-Packard gas chromatograph, model 5830A. The temperature uniformity of the oven was approximately ± 1°C.

An IBM PC microcomputer was used for data acquisition, with an analog-digital board (model DT2801), thermocouple analog interface board (model DT756-Y), and digital input-output board (model DT752) from Datatranslation. The output signal from the UV detector was digitized and saved every 0.125 s during a run. The data acquisition routine was initiated when the solute injector valve was turned.

The microcomputer was programmed to calculate maximum peak heights, peak variance, and mean retention times. The actual data shown in subsequent figures are $\epsilon(1 + k_i)$ since this quantity came directly from our measurements as described here. From Eq. 2,

$$\tau_i = \tau_0(1 + k_i)$$

$$\tau_0 \equiv \frac{L}{u} \tag{20}$$

where L is the bed length and u the superficial linear velocity of the mobile phase. Since the mass flow rate of the mobile phase is kept constant during a run, and temperature and pressure conditions of both the column and the surroundings are known, τ_0 can be stated as

$$\tau_0 = \frac{\epsilon AL}{(\dot{m}/\rho_{col})} \tag{21}$$

where $\dot{m}$ is mass flow rate of carrier phase, p_{col} is the density of the mobile phase in the column, and A is the cross-sectional area of the bed. Since the volumetric flow rate of the mobile phase is measured at ambient conditions in the dry test meter,

$$\dot{m} = \dot{Q}\rho_{\text{amb}} \tag{22}$$

where $\dot{Q}$ is flow rate and ρ_{amb} the density of the fluid at ambient conditions. Therefore using Eqs. 20, 21, and 22,

$$\frac{\tau_i \dot{Q}\rho_{amb}}{AL\rho_{col}} = \epsilon(1 + k_i) \tag{23}$$

All the quantities on the lefthand side of Eq. 23 are measured for each experiment, hence $\epsilon(1 + k_i)$ is the direct result of these data. The advantage of this approach is that the bed porosity is merely a multiplicative factor and need not be explicitly measured.

Fitting of experimental data

The detailed molecular model for the capacity factor developed in the Appendix resulted in Eq. A11, which we repeat below for the solute species at infinite dilution. (The justification for using the infinite dilution limit is that mole fractions of solutes in these systems are usually of the order 10^{-3} and lower).

$$k_b^{\infty} = \frac{\dfrac{K_0 \hat{\phi}_b^{\infty} p \Lambda_b^3}{\rho_m kT}\left(\dfrac{e^{-D_b/2T}}{1 - e^{-D_b/T}}\right)^3 e^{-U_b^0/kT}}{1 + \dfrac{\hat{\phi}_a p \Lambda_a^3}{kT}\left(\dfrac{e^{-D_a/2T}}{1 - e^{-D_a/T}}\right)^3 e^{-U_a^0/kT}} \tag{24}$$

There are a number of features of data reduction with this model that are worth discussing. The mobile phase requires the calculation of a fugacity coefficient for the solute species denoted by ϕ_b. For this an equation of state is required, parameters for which may be evaluated from solubility data for the particular solute in the supercritical solvent. Here we used the perturbed hard sphere model studied in our previous work (Chimowitz et al., 1988), in conjunction with the relevant solubility data. The stationary phase part of the model has a number of parameters. The Debye temperature D_i, defined as $h\upsilon/k$, is required for each type of molecule–site pair. Examination of bond vibrational frequency data shows that D_i for a wide variety of bonds lies within a relatively narrow range; as a result, D_i was established as 300 K for both species (Hill, 1962). The parameter U_i^0 reflects the well depth for the potential associated with the molecule–site interaction for species i. For the solvent molecule we establish its value based upon the following considerations. For pure solvent adsorption at reduced conditions $T_R \approx 1$ and $P_R \approx 2$, it is reasonable to assume that the majority of the sites are occupied by solvent molecules, that is, $\theta_a = 0.99$. The adsorption model in the Appendix can then be solved for this situation, yielding a value for U_a^0/k (here k is Boltzmann's constant). For carbon dioxide this produced a value of $-$ 5,835 K for U_a^0/k. The model has now been reduced to a single parameter model from which U_b^0/k may be found from capacity factor data for the system at hand. With further simplification it is possible to remove the packing term K_0. Equation 24 can be written in a simplified way, more explicit in the unknown parameters, as:

$$k_b = \frac{K_0 \cdot X \cdot e^{-U_b^0/kT}}{1 + Y} \tag{25}$$

with X and Y defined to be the respective terms in Eq. 24.

If we denote the datum for a given experiment as $g_i \equiv \epsilon(1 + k_i)$, then combining Eqs. 23 and 25 for the jth experiment:

$$g_j = \left[\epsilon\left(1 + \frac{K_0 \cdot X \cdot e^{-U_b^0/kT}}{1 + Y}\right)\right]_j \tag{26}$$

ϵ serves only to scale the data, and it was set at the value of 0.5 (accurate for the column used here). Therefore,

$$g_j^* \equiv \frac{1}{0.5} g_j - 1 = \left.\frac{K_0 \cdot X \cdot e^{-U_b^0/kT}}{1 + Y}\right]_j \tag{27}$$

From Eq. 27 it can be seen that K_0 is merely a multiplicative term, assumed constant for a given column, which can be removed by referring all data to a reference datum, ending up with what we call the relative capacity factor g_j^{**}:

$$g_j^{**} = \frac{g_j^*}{g_{ref}^*} = \frac{\left(\dfrac{X \cdot e^{-U_b^0/kT}}{1 + Y}\right)_j}{\left(\dfrac{X \cdot e^{-U_b^0/kT}}{1 + Y}\right)_{ref}} \tag{28}$$

and

$$g_j^{cal} = \frac{\left(\dfrac{X \cdot e^{-U_b^0/kT}}{1 + Y}\right)_j}{\left(\dfrac{X \cdot e^{-U_b^0/kT}}{1 + Y}\right)_{ref}} \quad \begin{matrix} \text{calculated at } T_j, P_j \\ \text{calculated at } T_{ref}, P_{ref} \end{matrix}$$

These then are the expressions we are after, containing only one parameter U_b^o per solvent–solute system. A simple one-dimensional search to yield an optimal U_b^o was applied to minimize an objective function of the form:

$$\phi(U_b^0) = \sqrt{\sum_{j=1}^{n} (g_j^{**} - g_j^{calc})^2}$$

The choice of the reference datum is arbitrary. For all the results that follow the reference datum was taken to be the first data point in each set.

Results

To study the ideas and model proposed in earlier sections three systems were chosen: 2,3-dimethylnaphthalene (DMN), 2,6-DMN, and naphthalene in supercritical carbon dioxide. Solubility data for each of these respective systems are available (Kurnik et al., 1981), which meant that the equation of state parameters could be fitted independently of the chromatographic data. In addition, the isomeric DMN system provided a

good test of the optimal resolution issue raised in a previous section.

Since the development of the theory required the assumption of equilibrium established between the mobile and stationary phases, the first series of experiments was designed to evaluate the accuracy of this assumption. Capacity factor data were measured at various flow rates in the system under the same conditions of temperature and pressure. Any deviation from equilibrium, resulting in a rate-controlled transfer process, should manifest as a change in capacity factors with increasing flow rates. This was established to be not the case, as can be seen from representative data for the 2,6-DMN experiments shown in Figure 2.

Experiments were then done to determine the effects of temperature and pressure on capacity factors for the three systems studied. These data are presented in Table 1 for 2,3-DMN–CO_2 and 2,6-DMN–CO_2, and in Table 2 for naphthalene–CO_2 at two different pressures and a series of temperatures. The data represent averages of at least three and often four experiments per temperature. The mobile-phase flow rates for these data were 30.59 ± 0.28 L/h. The optimal well depth parameters U_b^o fitted to the model as discussed previously are shown in Table 3.

Relative capacity factors were defined in an earlier section so as to eliminate column and packing parameters from the model. The capacity factor data in Tables 1 and 2 were fitted to the model and a comparison of the data and model calculations for the 91 bar data are shown in Figures 3 and 4 for 2,3-DMN and 2,6-DMN in supercritical carbon dioxide. The fit between data and the model was reasonably good for each system. Note that the model shows a strong increase in retention (capacity factor) for both systems beginning at approximately 320 K. A turning point is shown, after which the capacity factors decrease monotonically with increasing temperature for the temperature range studied. The model and data are entirely consistent with the analysis presented earlier, where it was shown how this behavior may be ascribed to the large exothermic energetic effects presented by solutes dissolved in near-critical fluids. Our previous analysis showed that the turning point for the model

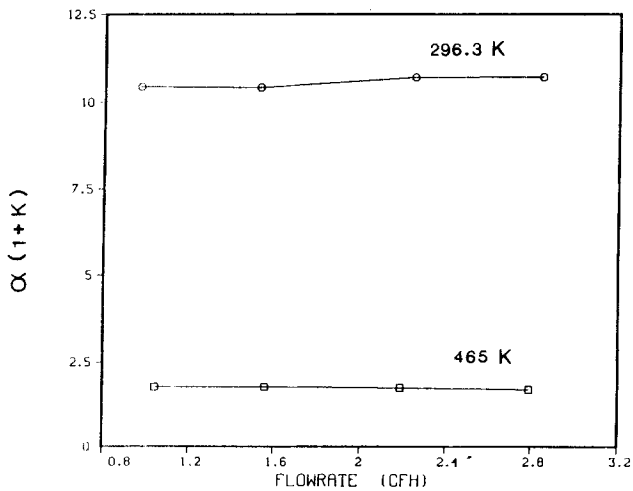

Figure 2. Data showing validity of equilibrium assumption.

Table 1. Capacity Factor Data DMN Isomeric System in Supercritical CO_2 at Two Pressures on an ODS Column

Press. bar	Temp. K	$\epsilon(1+k)$ 2,3-DMN	$\epsilon(1+k)$ 2,6-DMN
91.0	297.3	1.87	1.77
	304.4	1.27	2.12
	312.0	4.7	4.3
	319.0	17.6	15.54
	326.0	46.43	40.35
	376.6	62.56	54.4
	406.0	35.93	31.62
	435.9	19.95	17.8
	465.8	11.7	10.58
	496.2	7.27	6.68
	526.3	4.87	4.54
138.4	307.2	1.72	1.64
	317.8	2.03	1.91
	333.9	3.58	3.28
	346.8	6.75	6.08
	376.4	12.8	11.38
	406.5	11.78	10.53
	435.0	8.8	7.95
	464.5	6.18	5.66
	493.9	4.45	4.15

occurs at a temperature satisfying the following approximate equation derived from Eq. 15:

$$[(h_b^0 - \overline{h}_b^m) - (h_b^0 - \overline{h}_b^s)] + RT^2\alpha^m = 0 \qquad (29)$$

For carbon dioxide, for example, the value of α at conditions in the vicinity of the data shown is of the order of 0.012 K^{-1}. This makes the latter term in Eq. 29 of the order of 12–16 kJ/mol throughout most of the P-T region, quite insignificant in the

Table 2. Capacity Factor Data for Naphthalene in Supercritical CO_2 at Two Pressures on an ODS Column

Press. bar	Temp. K	$\epsilon(1+k)$
95.0	296.2	1.46
	308.0	1.9
	322.7	10.73
	337.8	25.5
	352.9	27.2
	367.4	23.86
	382.8	19.66
	413.2	12.37
	442.7	7.95
	472.2	5.42
135.9	294.8	1.32
	308.0	1.43
	322.7	1.81
	337.8	3.28
	352.9	5.6
	367.3	7.08
	382.9	7.35
	413.3	6.23
	442.8	4.8
	472.3	3.67

Table 3. Well Depth Parameters for Surface Molecule Species in Supercritical CO_2 on an ODS Column

	U_b^o/k	Press. bar
2,6-DMN	−12,204.9	91
2,3-DMN	−12,481.1	91
Naphthalene	−11,074.9	95

retrograde region compared to the solute energy term in Eq. 29. This implies that the temperatures that satisfy Eq. 29 will be close to the temperatures where the mobile-phase partial molar configurational enthalpy function intersects the solute surface enthalpy function. These matters can best be illustrated with the use of Figures 5 and 6. Figure 5 shows the calculated individual energy functions appearing in Eq 29, for 2,3-DMN in carbon dioxide at 91 bar pressure. Figure 6 shows the calculated capacity factor for 2,3-DMN in CO_2 at the same pressure, using the complete model. From Figure 5, as the temperature increases from 280 K a point is reached at which the difference in energy functions $(h_b^o - \bar{h}_b^m)$ and $(h_b^o - \bar{h}_b^s)$ equals the term $RT^2\alpha^m$ (see Eq. 29). This corresponds to a low-temperature region turning point T_{min} in Figure 6. With the onset of retrograde behavior in the system the solute partial molar configurational enthalpy function for the fluid phase shows a dramatic increase, corresponding to the steep increase in retention times and capacity factors seen in Figure 6. As the system moves beyond the retrograde region a similar condition arises between the various energy terms, leading to the high-temperature region turning point condition T_{max}, the maximum along the capacity factor trajectory. There is an expected small discrepancy between T_{max} given by Figures 5 and 6. The explanation for this lies in the fact that the exact model was used for the calculations of capacity factor in Figure 6, whereas the functions shown in Figure 5 represent only the dominant contributions to the temperature derivative of the capacity factor as given by Eq. 15. The effect of including the solvent term in Eq. 15 would be to shift the αRT^2 function upward, resulting in a widening of the temperature range between T_{min} and T_{max}, in agreement with the results of Figure 6. Nevertheless, the approximate analysis is a useful one, especially since there is almost a direct analogy

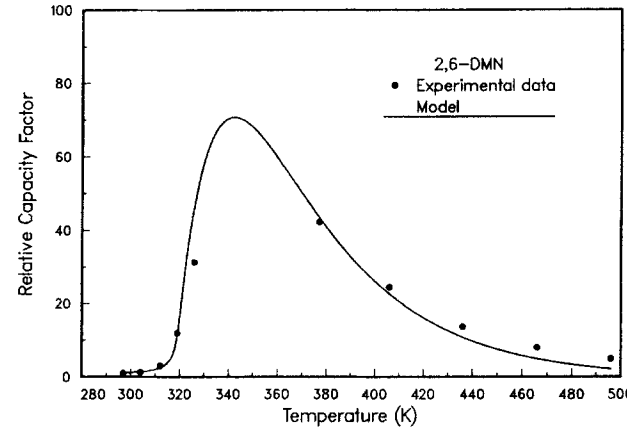

Figure 4. Experimental and calculated relative capacity factors for 2,6-DMN in CO_2 at 91 bar.

between this analysis for capacity factors and the discussion of retrograde solvation in supercritical fluids given by Chimowitz et al. (1988). This suggests that the large amount of published solubility data in supercritical fluids may be used to get an accurate picture of how the solute–solvent pair would behave in an entirely different process environment akin to a fixed-bed chromatographic mode.

The data for naphthalene and the model representation are presented in Figure 7 for 95 bar. Figure 8 shows data and the model predictions for the higher pressure experiments at 135 bar. The agreement between model and data is quite good for both sets of data. In particular, note how the strong dependence of retention time is much attenuated at the higher pressure conditions, where the mobile phase is much further removed from its critical point. In these circumstances the distinctions between SFC and both HPLC and gas chromatography begin to vanish. These results show that the model presented earlier appears to represent the data well, even in the highly compressible region where the capacity factor dependence on temperature is extremely strong. In comparison to the results of Yonker et al. (1985), this approach seems to provide a significant improvement (for the same number of adjustable model parameters), especially in the near-critical regime. A more stringent requirement for any model is its ability to be predictive of the

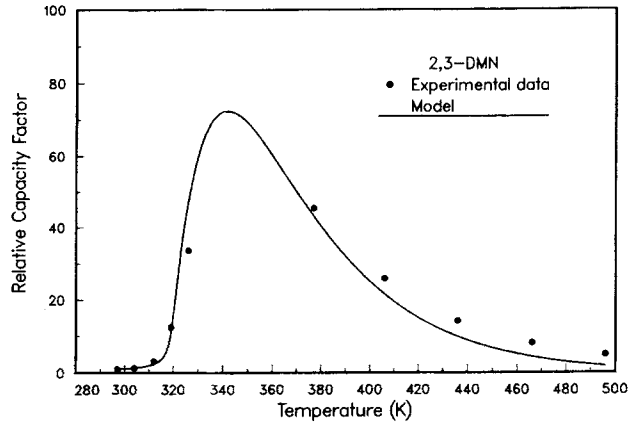

Figure 3. Experimental and calculated relative capacity factors for 2,3-DMN in CO_2 at 91 bar.

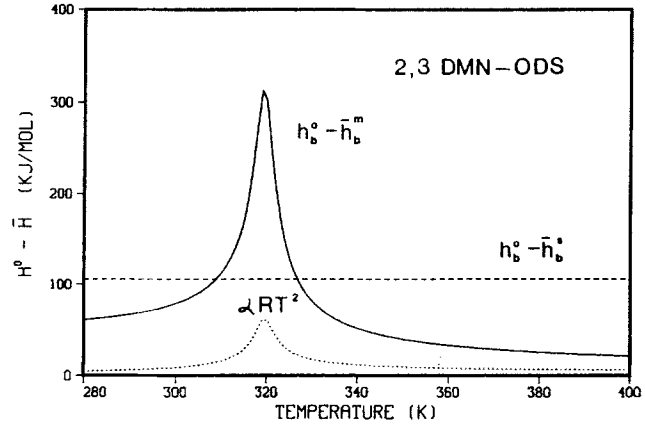

Figure 5. Individual energy terms in approximate equation for 2,3—DMN in CO_2.

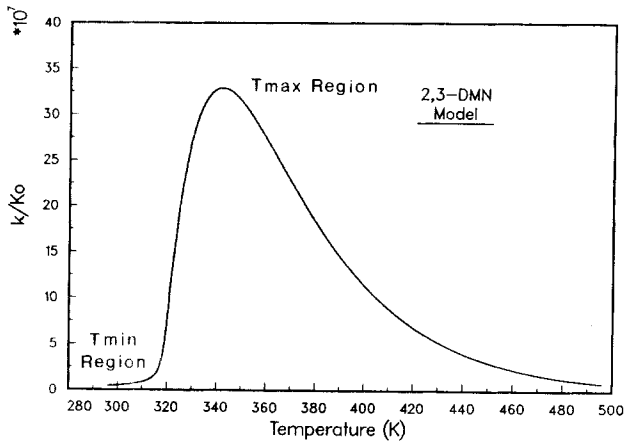

Figure 6. Calculated capacity factor envelope for 2,3-DMN in CO_2.

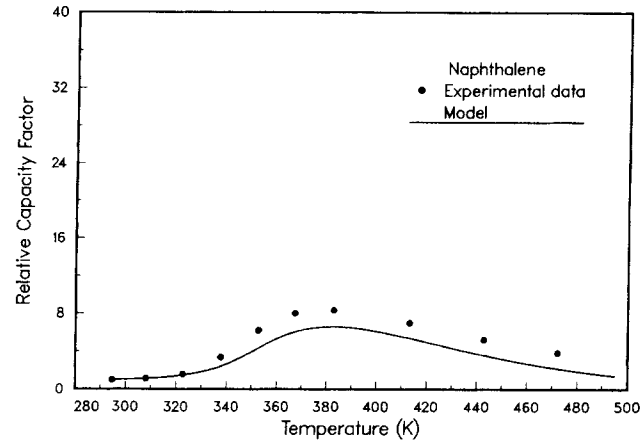

Figure 8. Model predictions at 135 bar for naphthalene in CO_2.

phenomena given pure-component molecular properties. For this model the single parameter required to make it predictive is U_b^o, reflective of the solute molecule–site well depth. It is natural to ask whether, for a given system, U_b^o correlates at all with a pure-component property of the solute molecule that itself reflects the forces between solute molecules. Such a quantity is the heat of sublimation or heat of vaporization. If the correlation is reasonable then the model becomes predictive. Given the pure solute's property, U_b^o can be found and the capacity factor envelope calculated. Clearly this should in principle be a different correlation for each surface phase–solvent system. We investigated this possibility and a plot showing results for the carbon dioxide–ODS system is shown in Figure 9, which contains additional information for the isomeric *o*-xylene, *p*-xylene, *m*-xylene system and toluene, for which additional data were acquired. While not conclusive, these results look encouraging in that such a correlation appears to be evident. Further work to see whether this result generalizes to other systems seems warranted.

The final aspect of this paper concerns the issue of molecular resolution and the potential significance of this work for molecular separations. It was pointed out earlier that the thermodynamic properties of the solute–fluid interaction are likely to be most different from each other in the near-critical region, even for structurally similar molecules. This region then takes on special significance from the point of view of molecular resolution. Experimentally, it can be studied by varying the mobile-phase molecular makeup for the same set of solute species or vice versa. We did both sets of experiments and chose ethane as the alternative solvent species since its critical termperature (305.4 K) is so close to that of carbon dioxide (304.2 K). Hence the same absolute temperatures imply virtually identical reduced temperatures for both solvent types. Experiments were done to determine capacity factors for the DMN isomers and naphthalene using the same ODS column in supercritical ethane. These data are given in Table 4. The pressures were chosen so as to be similar to the reduced pressures for the previously given data for supercritical carbon dioxide. More interesting are the data displayed in Figure 10, which shows the naphthalene data for both supercritical carbon dioxide and ethane at similar reduced pressures. It is evident that at both low and high temperature conditions the data tend to converge whereas strong divergence shows up in the region where the

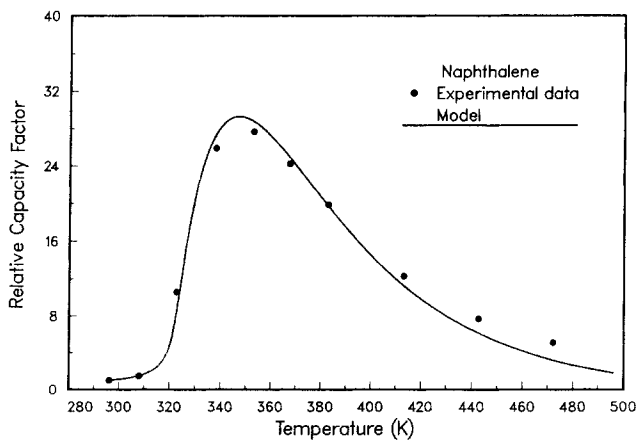

Figure 7. Experimental and calculated relative capacity factors for naphthalene in CO_2 at 95 bar.

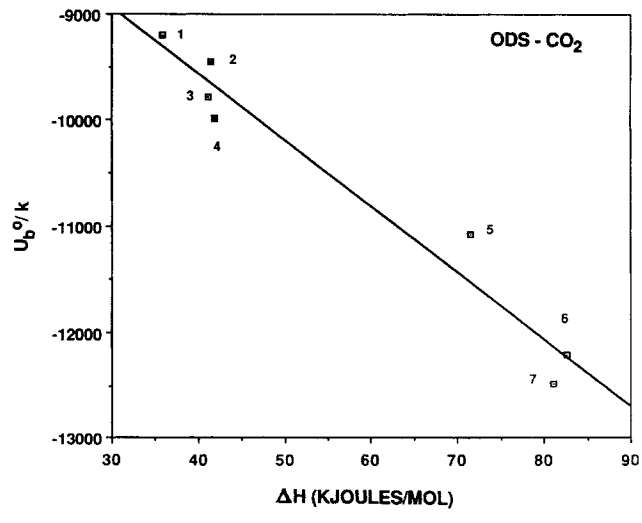

Figure 9. Correlation of U_b^o with a solute property.

1. Toluene; 2. *m*- xylene; 3. *p*-xylene; 4. *o*-xylene; 5. Naphthalene; 6. 2,6-DMN; 7. 2,3-DMN

Table 4. Capacity Factor Data for DMN Isomers and Naphthalene in Supercritical Ethane at a Reduced Pressure of 1.26 on an ODS Column

Press. bar	Temp. K	$\epsilon(1+k)$ 2,3-DMN	2,6-DMN	Naphthalene
61.0	295.5	2.07	1.88	1.72
	304.4	2.57	2.31	2.05
	312.0	3.92	3.47	2.88
	319.9	12.21	10.54	7.64
	326.2	33.28	28.27	17.35
	377.0	77.56	66.11	30.7
	406.7	43.46	37.67	18.44
	436.7	23.25	20.52	10.95
	466.5	13.23	11.86	6.97
	496.6	8.18	7.46	4.82

retrograde effect dominates. These data show that intermolecular differences are most pronounced in the near-critical region, consistent with our earlier hypothesis. The same can be said for both isomeric systems in both solvents. These data are shown in Figures 11 and 12 for 2,3-DMN and 2,6-DMN, respectively. The fact that this divergence is strongly diminished at higher pressures reaffirms the idea that it is the compressible, near-critical region where molecular selectivity is greatest. Data illustrating this for 2,3-DMN in both supercritical carbon dioxide and ethane at a higher reduced pressure of 1.89 are shown in Figure 13. The converse perspective alluded to earlier, that of different solutes in the same solvent, reveals interesting features. Figure 14 shows the difference in mean retention times for the 2,3-DMN, 2,6-DMN system in carbon dioxide. A dramatic increase is evident beginning at approximately 325 K, with a maximum value at approximately 345 K at 91 bar. From a thermodynamic standpoint this turning-point temperature represents the optimal separation point for this system at the prescribed pressure. It is unequivocally the condition at which the species difference in mean residence times will be a maximum, all other things being equal, (packing material, flow rates, column length, etc.). It is this ability to greatly influence resolution in the near-critical region that we believe holds

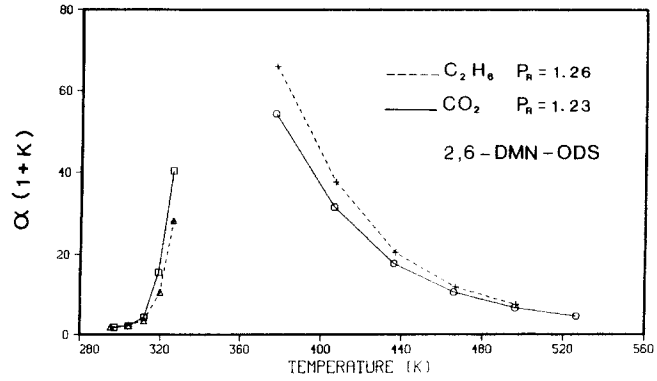

Figure 11. Data for 2,3-DMN in supercritical CO_2 and ethane.
Pressure: CO_2, 91 bar; ethane, 61 bar

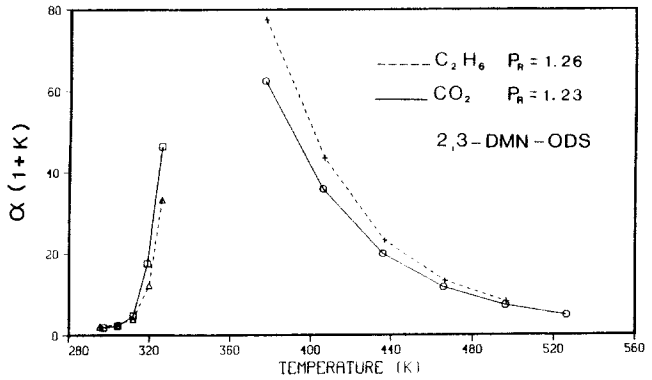

Figure 12. Data for 2,6-DMN in supercritical CO_2 and ethane.
Pressure: CO_2, 91 bar; ethane, 61 bar

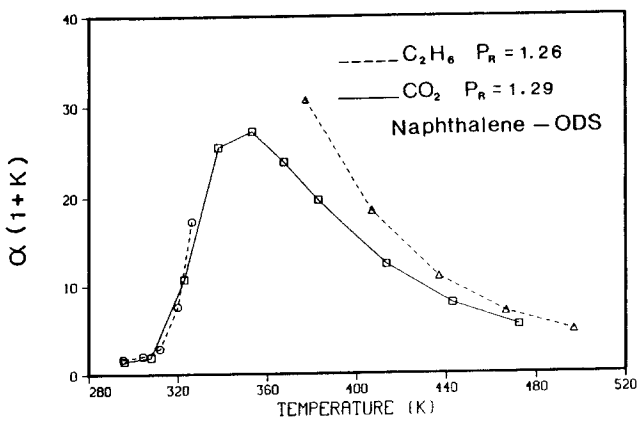

Figure 10. Data for naphthalene in supercritical CO_2 and ethane.
Pressure: CO_2, 95 bar; ethane, 61 bar

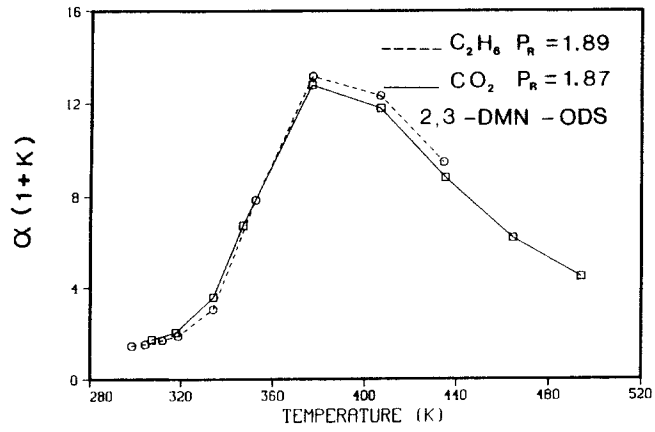

Figure 13. High-pressure data for 2,3-DMN in supercritical CO_2 and ethane.
Pressure: CO_2, 138 bar; ethane, 91.8 bar

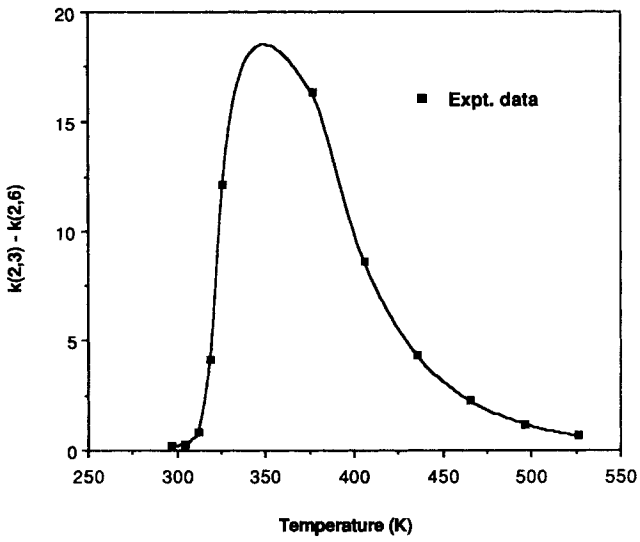

Figure 14. Data showing point of maximum resolution for DMN isomeric system in supercritical CO_2.

promise for further development of optimal SFC processes. While the results for the DMN system appear promising, there is still much to be understood. Similar data for the phenanthrene–anthracene–carbon dioxide system, for example, show only marginal increases in resolution over the capacity factor envelope.

Conclusions

This work has discussed the role of retrograde phenomena in the near-critical region on column retention behavior, molecular resolution, and capacity factor data in supercritical fluid chromatography. An equation to model and predict this complex behavior was proposed and shown to be quite accurate for representing the data presented. In fact, the model correlated the capacity factor data to the same degree of accuracy we have found using current equations of state to model solubility data alone in the near-critical region. In particular, the phenomenological features of the systems have been well represented. These include the strong increase in column retention times with the onset of retrograde behavior, turning points, and the subsequent asymmetric decline of capacity factors with increasing temperature. The relevance of the turning-point region as a domain of maximum resolution was discussed and illustrated with data from two solvent systems and solute systems that included an isomeric mixture. At the turning-point condition, while potential resolution is maximized, actual separation time often tends to be maximal since it is the point where species move slowly. Hence turning points are interesting features of the phenomena but merely initial conditions for what is an interesting optimal control problem in SFC.

Acknowledgment

The authors acknowledge financial support for this work provided by the National Science Foundation, Grant No. CBT 8704943.

Notation

A = bed cross-sectional area
C = factor in model
D = Debye temperature
f_i = fugacity, species i
h_i = enthalpy, species i
k = Boltzmann's constant
k_i = capacity factor, species i
K_0 = bed structure parameter
L = bed length
N = number of moles
P = pressure
q_i = bound molecule partition function
q_i^* = surface species concentration
Q = partition function
$\dot{Q}$ = flow rate
R = gas constant
T = temperature
u = mobile phase superficial velocity
U_b^o = well depth parameter species b
V_i = volume species i
y_i = mole fraction species i

Greek letters

α = volume expansivity
β = isothermal compressibility
Δ = determinant function
θ_i = fraction coverage, species i
ϵ = bed porosity
ϕ = fugacity coefficient
ρ = density
Ω = degeneracy factor
τ_i = residence time, species i
τ_0 = residence time, unretained species

Subscripts

a = solvent species
b = solute species
B = bulk phase
i = species i
m = mobile phase
o = ideal gas property
sub = sublimation

Superscripts

$-$ = partial molar property
s = surface phase species

Literature Cited

Brown, B. O., A. J. Kishbaugh, and M. E. Paulaitis, "Experimental Determination of Enhancement Factors from Supercritical Fluid Chromatography," *Fluid Phase Equil.*, **36**, 247 (1987).

Cassielles, A. G., C. Pando, J. A. R. Renuncio, J. J. Christensen, and R. M. Izatt, "Excess Enthalpies of the Ternary System CO_2 + *n*-Hexane + Toluene at Supercritical Conditions," *Int. Symp. on Supercritical Fluids, Oct. (1988), Nice*, **1**, 311, Societe Francaise de Chimie (1988)

Chimowitz, E. H., and F. D. Kelley, "A New Representation for Retention Time in Supercritical Fluid Chromatography," *J. Supercrit. Fluids*, **2**, 106 (1989).

Chimowitz, E. H., and K. P. Pennisi, "Process Synthesis Concepts for Supercritical Gas Extraction in the Crossover Region," *AIChE J.*, **32**, 1665 (1986).

Chimowitz, E. H., F. D. Kelley, and F. M. Munoz, "Analysis of Retrograde Behavior and the Crossover Effect in Supercritical Fluids," *Fluid Phase Equil.*, **44**, 23 (1988).

Debenedetti, P. G., and S. K. Kumar, "The Molecular Basis of Temperature Effects in Supercritical Extraction," *AIChE J.*, **34**, 645 (1988).

Eckert, C. A., D. H. Ziger, K. P. Johnston, and S. Kim, "Solute Partial Molar Volumes in Supercritical Fluids," *J. Phys. Chem.*, **90**, 2738 (1986).

Hill, T. L., *An Introduction to Statistical Thermodynamics,* 2d ed., Addison-Wesley, Reading, MA (1962).
Johnston, K. P., S. E. Barry, N. K. Read, and T. R. Holcomb, "Separation of Isomers Using Retrograde Crystallization from Supercritical Fluids," *Ind. Eng. Chem. Res.*, **26,** 2372 (1987).
Kelley, F. D., and E. H. Chimowitz, "Experimental Data for the Crossover Process in a Model Supercritical System," *AIChE J.*, **35,** 981 (1989).
Klesper, E., and F. P. Schmitz, "Gradient Methods in Supercritical Fluid Chromatography," *Supercrit. Fluids,* **1,** 45, (1988).
Kurnik, R. T., S. J. Holla, and R. C. Reid, "Solubility of Solids in Supercritical Carbon Dioxide and Ethylene," *J. Chem. Eng. Data,* **26,** 47 (1981).
Modell, M., and R. C. Reid, *Thermodynamics and Its Applications,* 2d ed. Prentice-Hall, Englewood Cliffs, NJ (1983).
Recasens, F., B. J. McCoy, and J. M. Smith, "Desorption Processes: Supercritical Fluid Regeneration of Activated Carbon," *AIChE J.*, **35,** 951 (1989).
Schaeffer, S. T., L. H. Zalkow, and A. Teja, "Supercritical Extraction of Crotalaria Spectabilis in the Crossover Region," *AIChE J.*, **34,** 1740 (1988).
Schmitz, F. P., D. Leyendecker, and E. Klesper, "Chromatography with Mobile Phases in the Liquid and the Supercritical State," *Ber. Bunsenges Phys. Chem.*, **88,** 912 (1984).
Sherwood, T. K., R. L. Pigford, and C. R. Wilke, *Mass Transfer,* McGraw-Hill, New York (1975).
Shim, J. J., and K. P. Johnston, "Adjustable Solute Distribution Between Polymers and Supercritical Fluids," *AIChE J.*, **35,** 1097 (1989).
Van Wasen, U., I. Swaid, and G. M. Schneider, "Physicochemical Principles and Applications of Supercritical Fluid Chromatography (SFC)," *Ang. Chemie, Int. Ed.*, **19,** 575 (1980).
Wong, J. M., J. S. Pearlman, and K. P. Johnston, "Supercritical Fluid Mixtures: Predictive of the Phase Behavior," *J. Phys. Chem.*, **89,** 2671 (1985).
Yonker, C. R., B. W. Wright, R. C. Peterson, and R. D. Smith, "Temperature Dependence of Retention in Supercritical Fluid Chromatography," *J. Phys. Chem.*, **89,** 5526 (1985).
Yonker, C. R., R. W. Wright, S. L. Frye, and R. D. Smith, "Mechanism of Solute Retention in Supercritical Fluid Chromatography," *Supercritical Fluids: Chemical and Engineering Principles and Applications,* Squires and Paulaitis, eds., ACS Symp. Ser., **329,** ch. 14 (1987).

Appendix

Starting with the capacity factor defined as

$$k_i = \frac{\text{number of moles if } i \text{ in the stationary phase}}{\text{number of moles if } i \text{ in the mobile phase}}$$

the following expression is valid for Langmuirian adsorption:

$$k_i = \frac{\theta_i M^* (1 - \epsilon)}{y_i \rho_m \epsilon} \tag{A1}$$

where M^* is the total concentration of sites available in a representative slice of the packed bed, and θ_i is the fraction of those sites occupied by species i. The appropriate unit for M^* is moles of sites per unit volume.

The surface of a solid adsorbent is considered to be a lattice, where individual molecules can bind at the lattice sites. In the fluid phase there are N different molecular species. Each surface site is assumed to be capable of interacting with only one molecule at a time, and is independent of all the other sites. Therefore $N + 1$ surface sites types must be considered; N that are associated with molecules and sites that are unoccupied. When a site is occupied by a molecule of species i, the site has a partition function of q_i. Assuming that M sites exist on the solid, the canonical partition function can be written (Hill, 1962):

$$Q(T, M, N_1, N_2, \ldots, N_N) = \Omega(M, N_1, N_2, \ldots, N_N)\Pi_{i=1}^{N} q_i^{N_i}$$

where N_i is the number of i molecules on the surface, and Ω is the configurational degeneracy. For this model,

$$\Omega = \frac{\left(\sum_{i=1}^{N+1} N_i\right)!}{\prod_{i=1}^{N+1} (N_i!)} = \frac{M!}{\left(\prod_{i=1}^{N} N_i!\right)\left(M - \sum_{i=1}^{N} N_i\right)!}$$

where $N_{N+1} = M - \Sigma_{i=1}^{N} N_i$ is the number of unoccupied sites. Substituting this into the canonical ensemble yields

$$Q = \frac{M! \prod_{i}^{N} q_i^{N_i}}{\left(\prod_{i}^{N} N_i!\right)\left(M - \sum_{i}^{N} N_i\right)!} \tag{A2}$$

The chemical potential of a species is related to the canonical ensemble by:

$$-\frac{\mu_j}{kT} = -\ln \lambda_j = \left(\frac{\partial \ln Q}{\partial N_j}\right)_{T,M,N_{a \neq j}} \tag{A3}$$

Here λ_j is an absolute activity. The quantity M^* multiplied by the volume of the adsorbent equals M.

Using Eqs. A2 and A3 it can be shown that

$$(\lambda_j q_j)^{-1} = \frac{M - \sum_{i=1}^{N} N_i}{N_j} = \frac{N_{N+1}}{N_j}$$

The fractional surface coverage for species i is defined as

$$\theta_i = \frac{N_i}{M} = \frac{\lambda_i q_i N_{N+1}}{M} = \frac{\lambda_i q_i}{1 + \sum_{j=1}^{N} \lambda_j q_j} \tag{A4}$$

Equation A4 is the Langmuirian expression for surface coverage for the general case of N components adsorbing.

For the bound molecule partition function we used the analogy with molecules bound in a crystal lattice, where the molecular partition function is given by

$$q_i = q_x q_y q_z e^{-U^o/kT} \tag{A5}$$

where q_x, q_y, q_z are vibrational partition functions in the x, y, z, directions, k is Boltzmann's constant, and U^o is the depth of the well for the bound species–site interaction potential. Assuming an isotropic potential, q_{mol} then becomes

$$q_i = (q_{vib})^3 e^{-U^o/kT} \tag{A6}$$

Exact solutions for q_{vib} are available (Hill, 1960) in terms of the Debye temperature D_i defined as $D_i \equiv hv/k$ where v is the vibrational frequency and h is Planck's constant.

Since this is an equilibrium situation, the absolute activity N_i can be evaluated by using the chemical potential of the species in the gas phase.

Using a reference state of $f_i^o = p = 1$ atm for the fluid phase, the chemical potential of species i, μ_i, can be expressed as

$$\mu_i = \mu_i^o + kT \ln f_i = \mu_i^o + kT \ln (y_i \phi_i p) \tag{A7}$$

where f_i and ϕ_i are the fugacity and fugacity coefficient of i, respectively. Substituting this into the lefthand side of Eq. A3 yields

$$\lambda_i = y_i \phi_i p e^{\mu_i^o/kT} \tag{A8}$$

Since the reference state is an ideal gas, statistical mechanics can be used to find the function μ_i^o. For an ideal gas

$$Q = \frac{1}{N!}\left(\frac{V}{\Lambda^3}\right)^N$$

with

$$\Lambda = \frac{h}{(2\pi mkT)^{1/2}} \tag{A9}$$

where V is the volume, N is the number of molecules, and m is the molecular mass. Using Eq. A3 and the ideal gas equation of state it is easy to show that

$$\mu_i^o = -kT \ln\left(\frac{kT}{\Lambda_i^3}\right) \tag{A10}$$

In Eq. A10, Λ_i is the thermal de Broglie wavelength for species i.

For this simple case of an independent site lattice an analytic expression for k_i can be found, leading to:

$$k_i = \frac{\dfrac{\phi_i p \Lambda_i^3}{\rho_m kT} K_0 \left(\dfrac{e^{-D_i/2T}}{1 - e^{-D_i/T}}\right)^3 e^{-U_i^o/kT}}{1 + \sum_{j=1}^{N} \tau_j} \tag{A11}$$

where the τ_j are given as

$$\tau_j = \frac{y_j \phi_j p \Lambda_j^3}{kT} \left(\frac{e^{-D_j/2T}}{1 - e^{-D_j/T}}\right)^3 e^{-U_j^o/kT} \tag{A12}$$

In Eq. A11, K_0 is a bed structure parameter composed of only the geometric parameters that appear in the other equations. Consistency between Eqs. A11, 6 and 7 requires U_i^o to be considered a function of pressure. However, for data U_j^o/kT correlation (Eq. A11) is satisfactory since U_i^o is merely a model parameter.

Manuscript received Nov. 20, 1989, and revision received May 29, 1990.